A general heat transfer correlation for non-boiling gas–liquid flow with different flow patterns in horizontal pipes

Jae-yong Kim, Afshin J. Ghajar *

School of Mechanical and Aerospace Engineering, Oklahoma State University, Stillwater, OK 74078, USA

Received 2 June 2005; received in revised form 19 January 2006

Abstract

A general heat transfer correlation for non-boiling gas–liquid flow with different flow patterns in horizontal pipes is proposed. In order to overcome the effect of flow pattern on heat transfer, a flow pattern factor (effective wetted-perimeter) is developed and introduced into our proposed correlation. To verify the correlation, local heat transfer coefficients and flow parameters were measured for air–water flow in a pipe in the horizontal position with different flow patterns. The test section was a 27.9 mm ID stainless steel pipe with a length to diameter ratio of 100. A total of 114 data points were taken by carefully coordinating the liquid and gas superficial Reynolds number combinations. The heat transfer data were measured under a uniform wall heat flux boundary condition ranging from about 3000 W/m² to 10,600 W/m². The superficial Reynolds numbers ranged from about 820 to 26,000 for water and from about 560 to 48,000 for air. These experimental data including different flow patterns were successfully correlated by the proposed general two-phase heat transfer correlation with an overall mean deviation of 5.5%, a standard deviation of 11.7%, and a deviation range of −18.3% to 37.0%. Ninety three percent (93%) of the data were predicted within ±20% deviation.
© 2006 Elsevier Ltd. All rights reserved.

Keywords: Two-phase; Gas–liquid; Horizontal flow; Flow patterns; Heat transfer; Correlation

1. Introduction

Two-phase flows are commonly found in many industrial processes. The expression of 'two-phase flow' is used to describe the simultaneous flow of a gas and a liquid, a gas and a solid, two different liquids, or a liquid and a solid. Among these types of two-phase flow, gas–liquid flow has the most complexity due to the deformability and the compressibility of the phases. This study is concerned exclusively with non-boiling gas–liquid flow in pipes. This type of flow is commonly observed in many industrial applications, such as oil wells and pipelines, solar collectors, chemical reactors, and nuclear reactors, and its hydrodynamic and thermal

conditions are dependent upon the interaction between the two phases. Therefore, it is very important to understand heat transfer in gas–liquid two-phase flow for economical design and optimized operation in those industrial applications.

Numerous heat transfer experimental data and correlations for non-boiling forced convective heat transfer during gas–liquid two-phase flow in horizontal and vertical pipes with different flow patterns and fluid combinations have been published over the past 50 years and a brief review of these studies is given in the next section. Based on the shortcomings of the available work in the open literature, the study presented here was undertaken. The objectives of this study were to systematically gather quality gas–liquid non-boiling flow heat transfer data for a variety of flow patterns in a horizontal pipe. Use the data to better understand the non-boiling two-phase flow heat transfer behavior in horizontal pipes with respect to different flow patterns. Finally, develop a robust heat transfer correlation to predict non-boiling two-phase flow heat transfer in horizontal pipes for a variety of flow patterns.

2. A brief review of the related work

A comprehensive discussion of the available heat transfer experimental data and correlations for non-boiling forced convective heat transfer during gas–liquid two-phase flow in horizontal and vertical pipes with different flow patterns and fluid combinations has been provided by Kim et al. (1999). In their extensive literature search a total of 38 two-phase heat transfer correlations were identified. The validity of these correlations and their ranges of applicability were documented by the original authors. However, in most cases, the identified heat transfer correlations were based on a small set of experimental data with a limited range of variables and liquid–gas combinations. In order to further assess the validity of the identified correlations, Kim et al. (1999) compared the correlations against seven extensive sets of two-phase flow heat transfer experimental data available from the literature, for vertical and horizontal tubes and different flow patterns and fluids. Kim et al. (1999) for consistency, based the validity of the identified heat transfer correlations on the comparison between the predicted and experimental two-phase heat transfer coefficients meeting the ±30% criterion. A total of 524 data points from the available experimental studies were used for these comparisons. The experimental data included five different liquid–gas combinations (water–air, glycerin–air, silicone–air, water–helium, water–Freon 12), and covered a wide range of variables, including liquid and gas flow rates and properties, flow patterns, pipe sizes, and pipe orientation. Five of these experimental data sets are concerned with a wide variety of flow patterns in vertical pipes (a total of 455 data points) and the other two data sets are for limited flow patterns (slug—21 data points and annular—48 data points) within horizontal pipes. Kim et al. (1999) reported the results of their extensive comparisons in tabular form. They tabulated the recommended correlations according to flow orientations (vertical and horizontal), flow regimes (major flow patterns and transition flow patterns), and fluid combinations. Based on their study, Kim et al. (1999) concluded that there was no single correlation capable of predicting the non-boiling heat transfer in gas–liquid two-phase flow for all fluid combinations, flow patterns, flow regimes, and pipe orientations.

In a subsequent study, Kim et al. (2000) addressed some of the shortcomings identified by Kim et al. (1999) in their earlier study. In order to improve the prediction of heat transfer rate in non-boiling two-phase flow, regardless of fluid combination, flow pattern, and pipe orientation, a new correlation was developed by Kim et al. (2000). The correlation uses a carefully derived heat transfer model which takes into account the appropriate contributions of both the liquid and gas phases using the respective cross-sectional areas occupied by the two phases. Their proposed new correlation is

$$h_{TP} = (1-\varepsilon)h_L\left\{1 + C\left[\left(\frac{x}{1-x}\right)^m\left(\frac{\varepsilon}{1-\varepsilon}\right)^n\left(\frac{Pr_G}{Pr_L}\right)^p\left(\frac{\mu_G}{\mu_L}\right)^q\right]\right\} \tag{1}$$

where h_{TP} is overall mean two-phase heat transfer coefficient, h_L is heat transfer coefficient for liquid (evaluated as if only liquid phase alone were flowing), ε is void fraction defined as $A_G/(A_L + A_G)$ and A is pipe cross-sectional area, x is flow quality defined as $\dot{m}_G/(\dot{m}_L + \dot{m}_G)$ and $\dot{m}$ is mass flow rate, Pr is Prandtl number, μ is viscosity, C is the lead coefficient in the correlation, and m, n, p, and q are the constant exponents of the key parameters in Eq. (1) which have been expressed by a power-law relationship. The subscripts, L and G designate liquid and gas, respectively.

Kim et al. (2000) initially used their proposed heat transfer correlation, Eq. (1), to predict non-boiling two-phase heat transfer for turbulent flow ($Re_{SL} > 4000$, where Re_{SL} is the superficial liquid Reynolds number) in vertical pipes with different flow patterns and fluid combinations. They used 255 vertical pipe experimental data points from the literature to determine the different constants in their proposed correlation. Their proposed heat transfer correlation successfully predicted the experimental data with an overall absolute mean deviation of about 2.5% and an rms deviation of about 12.8%. The correlation, Eq. (1), with one set of constants (C, m, n, p, q) predicted about 83% of the data (212 data points) within ±15% deviation, and about 96% of the data (245 data points) within ±30% deviation.

Kim and Ghajar (2002) extended the predictive capability of their proposed heat transfer correlation, Eq. (1), to horizontal pipe flow. For this purpose they collected 150 air–water experimental data points for different flow patterns in their two-phase flow heat transfer laboratory. Eq. (1) successfully predicted their horizontal pipe experimental data with an absolute mean deviation of about 1.0% and an rms deviation of about 12%. The correlation predicted about 93% of the data (139 data points) within ±20% deviation. The determined constants (C, m, n, p, q) and the ranges of parameters are shown in Table 1. As shown in this table, the correlation of Kim et al. (2000), Eq. (1), does an excellent job of predicting the limited horizontal pipe flow experimental data for the individual flow patterns. However, the correlation uses a different set of constants for each flow pattern and it is not capable, with good accuracy, to predict the heat transfer data for all the flow patterns with the same set of constants (C, m, n, p, q).

From the study of Kim and Ghajar (2002) and the results presented in Table 1, it is apparent that the non-boiling two-phase flow heat transfer in horizontal pipes is strongly flow pattern dependent. In order for a heat transfer correlation, such as Eq. (1), to be successful in capturing the dependency of the heat transfer data on the flow pattern, we need a much larger data base that accurately represents the flow behavior from one flow pattern to the next. No such data base is currently available in the open literature for the horizontal pipe flow. The only non-boiling two-phase flow heat transfer data in horizontal pipes available in the open literature are the recent data (150 data points) of Kim and Ghajar (2002) for different flow patterns (slug, wavy, slug-transition, and annular-transition) and the antiquated data of King (1952) for slug flow (21 data points) and Pletcher (1966) for annular flow (48 data points).

3. Experimental setup and data reduction

A schematic diagram of the overall experimental setup for heat transfer and flow visualizations in two-phase air–water flow in a horizontal pipe is shown in Fig. 1. The test section is a 27.9 mm ID straight standard stainless steel schedule 10S pipe with a length to diameter ratio of 100. The setup rests atop an aluminum I-beam that is supported by a pivoting foot and a stationary foot that incorporates a small electric screw-jack. The I-beam is approximately 9 m in length and can be inclined to an angle of approximately 8° above horizontal.

Table 1
Determined constants and range of parameters of Kim and Ghajar (2002) non-boiling heat transfer correlation for horizontal gas–liquid flow

| Flow patterns (no. of data points)	Value of constants					Range of parameters				
	C	m	n	p	q	Re_{SL}	$\left(\frac{x}{1-x}\right)$	$\left(\frac{\varepsilon}{1-\varepsilon}\right)$	$\left(\frac{Pr_G}{Pr_L}\right)$	$\left(\frac{\mu_G}{\mu_L}\right)$
Slug, bubbly/slug, bubbly/slug/annular (89 data points)	2.86	0.42	0.35	0.66	−0.72	2468 to 35503	6.9×10^{-4} to 0.03	0.36 to 3.45	0.102 to 0.137	0.015 to 0.028
Wavy-annular (41 data points)	1.58	1.40	0.54	−1.93	−0.09	2163 to 4985	0.05 to 0.13	3.10 to 4.55	0.10 to 0.11	0.015 to 0.018
Wavy (20 data points)	27.89	3.10	−4.44	−9.65	1.56	636 to 1829	0.08 to 0.25	4.87 to 8.85	0.102 to 0.107	0.016 to 0.021
All 150 data points	See above for the values for each flow pattern					636 to 35503	6.9×10^{-4} to 0.25	0.36 to 8.85	0.102 to 0.137	0.015 to 0.028
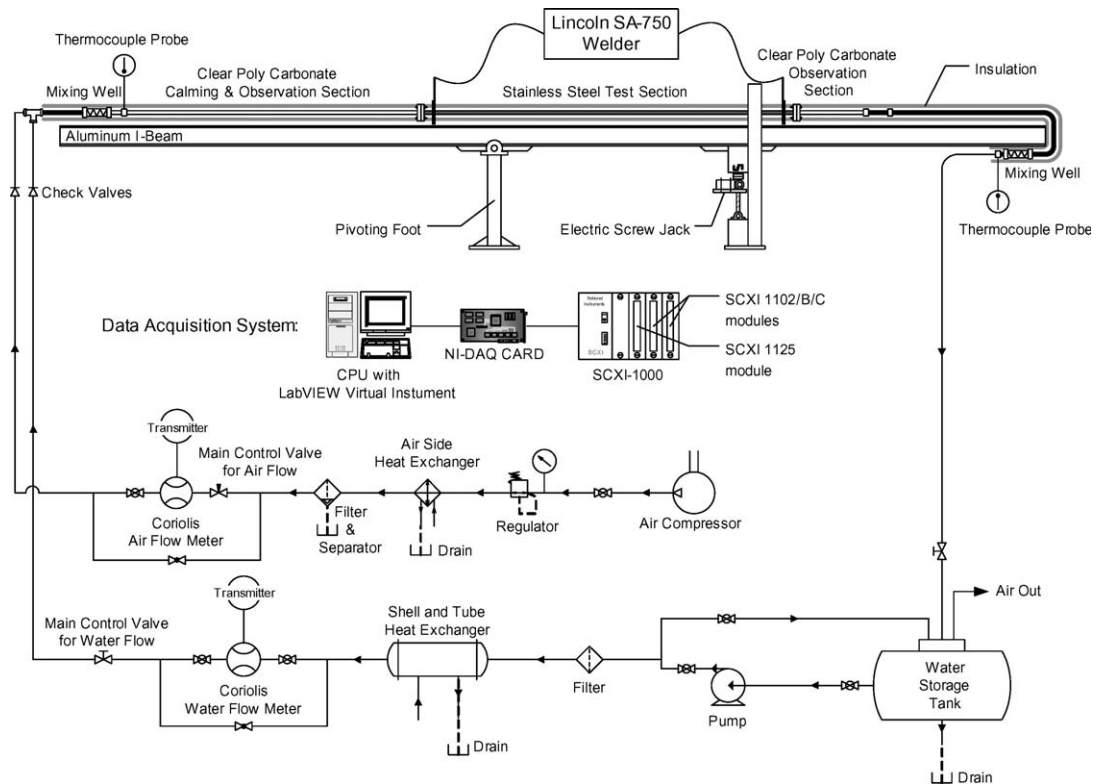
Fig. 1. Schematic diagram of the experimental setup.

In order to apply uniform wall heat flux boundary conditions to the test section, copper plates were silver soldered to the inlet and exit of the test section. The uniform wall heat flux boundary condition was maintained by a Lincoln SA-750 welder. The entire length of the test section was wrapped using fiberglass pipe wrap insulation, followed by a thin polymer vapor seal to prevent moisture penetration.

In order to develop various two-phase flow patterns (by controlling the flow rates of gas and liquid), a two-phase gas and liquid flow mixer was used. The mixer consisted of a perforated stainless steel tube (6.35 mm ID) inserted into the liquid stream by means of a tee and a compression fitting. The end of the copper tube was silver-soldered. Four holes (3 rows of 1.59 mm, 4 rows of 3.18 mm, and 8 rows of 3.97 mm) were positioned at 90° intervals around the perimeter of the tube and this pattern was repeated at fifteen equally spaced axial locations along the length of the stainless steel tube (refer to Fig. 2). The two-phase flow leaving the mixer entered the transparent calming section. The calming section [clear polycarbonate pipe with 25.4 mm ID and $L/D = 88$] served as a flow developing and turbulence reduction device, and flow pattern observation section.

T-type thermocouple wires were cemented with Omegabond 101, an epoxy adhesive with high thermal conductivity and electrical resistivity, to the outside wall of the stainless steel test section (refer to Fig. 3). Omega EXPP-T-20-TWSH extension wires were used for relay to the data acquisition system. Thermocouples were placed on the outer surface of the tube wall at uniform intervals of 254 mm from the entrance to the exit of the test section. There were 10 thermocouple stations in the test section. All stations had four thermocouples, and they were labeled looking at the tail of the fluid flow with peripheral location 'A' being at the top of the tube, 'B' being 90° in the clockwise direction, 'C' at the bottom of the tube, and 'D' being 90° from the bottom in the clockwise sense (refer to Fig. 3). The inlet liquid and gas temperatures and the exit bulk temperature were measured by Omega TMQSS-125U-6 thermocouple probes. To ensure a uniform fluid bulk temperature at the inlet and exit of the test section, a mixing well was utilized. An alternating polypropylene baffle type static mixer for both gas and liquid phases was used for the mixing well. This mixer provided an
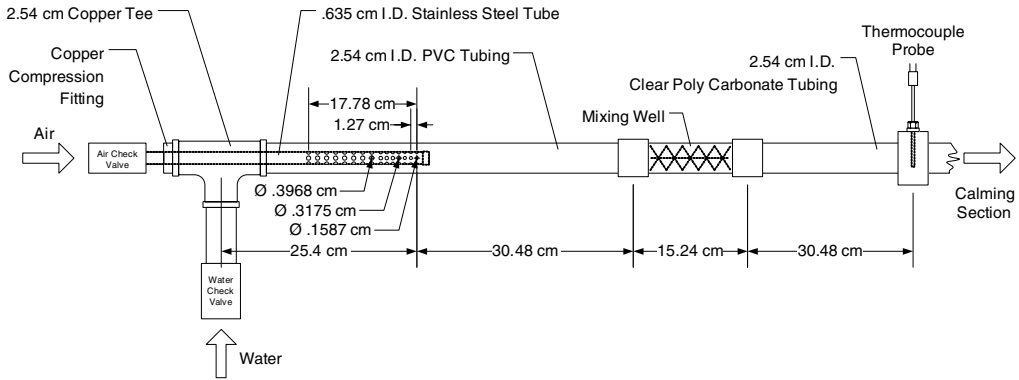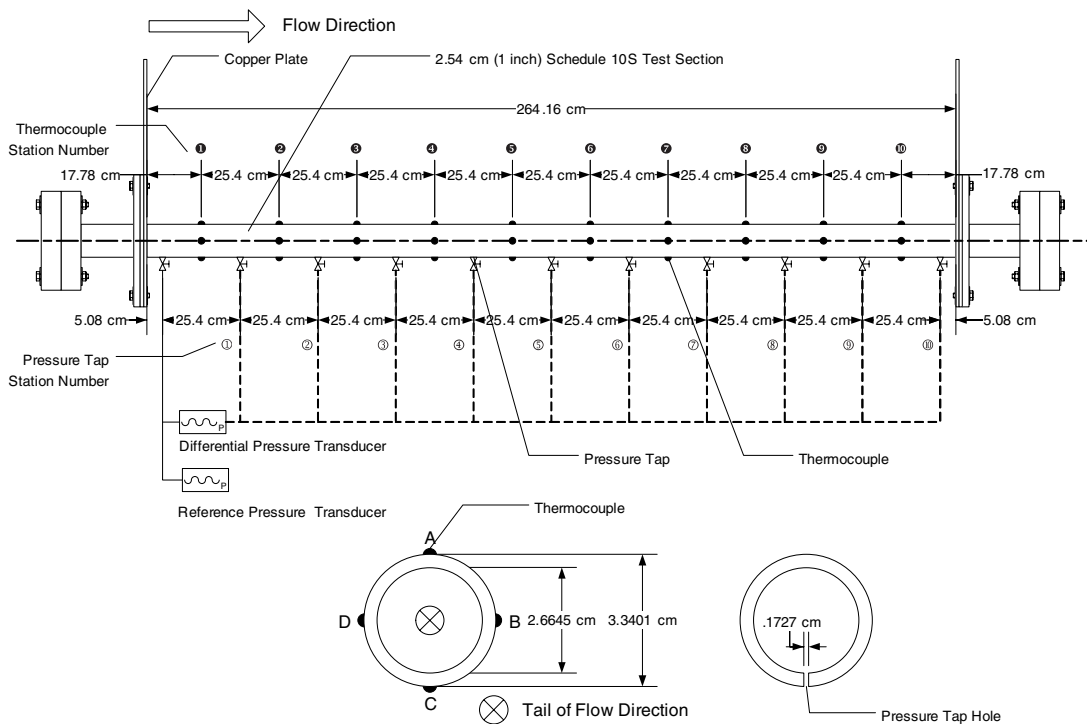
Fig. 2. Air–water mixing section.

Fig. 3. Test section.

overlapping baffled passage forcing the fluid to encounter flow reversal and swirling regions. The mixing well at the exit of the test section was placed below the clear polycarbonate observation section (after the test section), and before the liquid storage tank (refer to Fig. 1).

The fluids used in the test loop were air and water. The water was distilled and stored in a 55-gallon cylindrical polyethylene tank. A Bell & Gosset series 1535 coupled centrifugal pump was used to pump the water through a water filter. An ITT Standard model BCF 4063 one shell and two-tube pass heat exchanger removes the pump heat and the heat added during the test to maintain a constant inlet water temperature. From the heat exchanger, the water passes through a Micro Motion Coriolis flow meter (model CMF125) connected to a digital Field-Mount Transmitter (model RFT9739) that conditions the flow information for the data acquisition system. Once the water passes through the Coriolis flow meter it then passes through a 25.4 mm, 12-turn gate valve that regulates the amount of flow that entered the test section. From this point, the water travels

through a 25.4 mm flexible hose, through a one-way check valve, and into the test section. Air is supplied via an Ingersoll-Rand T30 (model 2545) industrial air compressor mounted outside the laboratory and isolated to reduce vibration onto the laboratory floor. The air passes through a copper coil submerged in a vessel of water to adjust the temperature of the air to room temperature. The air is then filtered and condensate removed in a coalescing filter. The air flow is measured by a Micro Motion Coriolis flow meter (model CMF100) connected to a digital Field-Mount Transmitter (model RFT9739) and regulated by a needle valve. Air is delivered to the test section by flexible tubing. The water and air mixture is returned to the reservoir where it is separated and the water recycled.

The heat transfer measurements at uniform wall heat flux boundary condition were carried out by measuring the local outside wall temperatures at 10 stations along the axis of the tube and the inlet and outlet bulk temperatures in addition to other measurements such as the flow rates of gas and liquid, system pressure, room temperature, voltage drop across the test section, and current carried by the test section. The peripheral heat transfer coefficient (local average) were calculated based on the knowledge of the pipe inside wall surface temperature and inside wall heat flux obtained from a data reduction program developed exclusively for this type of experiments by Ghajar and Zurigat (1991) and Ghajar and Kim (2006). The local average peripheral values for inside wall temperature, inside wall heat flux, and heat transfer coefficient were then obtained by averaging all the appropriate individual local peripheral values at each axial location.

Fig. 4 shows the typical temperature readings in two-phase flow from the thermocouples along the test section and the thermocouple probes at the inlet and outlet of the test section. The measurements shown in Fig. 4 are for slug flow with a superficial liquid Reynolds number of $Re_{SL} = 11{,}956$, a superficial gas Reynolds number of $Re_{SG} = 4937$, and a uniform wall heat flux of $\dot{q}'' = 8911$ W/m^2. The top thermocouples (curve 'A' in Fig. 4, refer to Fig. 3 for the thermocouple locations) along the test section indicated the highest temperature and the bottom thermocouples (curve 'C' in Fig. 4) indicated the lowest temperature readings. The variation in the circumferential wall temperature distribution, which is typical for two-phase gas–liquid flow in horizontal pipes, leads to different heat transfer coefficients depending on which circumferential wall temperature was selected for the calculations. In two-phase heat transfer experiments, in order to overcome the unbalanced circumferential heat transfer coefficients and to get a representative heat transfer coefficient for a test run, Eq. (2) was used to calculate an overall mean two-phase heat transfer coefficient (h_{TP}) for each test run

$$h_{TP} = \frac{1}{L} \int \bar{h}\,\mathrm{d}z = \frac{1}{L} \sum_{k=1}^{N_{ST}} \bar{h}_k \Delta z_k = \frac{1}{L} \sum_{k=1}^{N_{ST}} \left(\frac{\overline{\dot{q}}''}{\overline{T}_w - T_b} \right)_k \Delta z_k \tag{2}$$
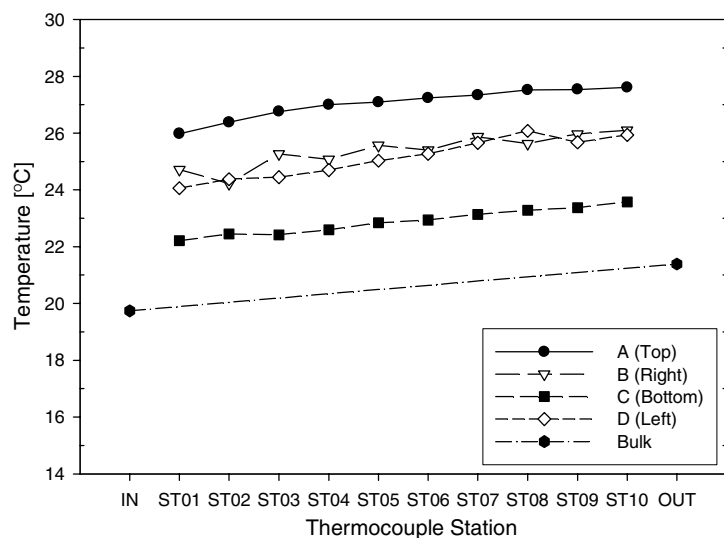

Fig. 4. Typical temperature readings in two-phase gas–liquid flow in a horizontal pipe. The case shown is for slug flow with $Re_{SL} = 11{,}956$, $Re_{SG} = 4937$, and $\dot{q}'' = 8911$ W/m^2.

where L is the length of the test section, $\bar{h}$, $\overline{q}''$, $\bar{T}_w$, T_b are the local mean heat transfer coefficient, the local mean heat flux, the local mean wall temperature, and the bulk temperature at a thermocouple station, respectively; k is the index of the thermocouple stations, N_{ST} is the number of the thermocouple stations, z is the axial coordinate, and Δz is the element length of each thermocouple station.

The data reduction program used a finite-difference formulation to determine the inside wall temperature and the inside wall heat flux from measurements of the outside wall temperature, the heat generation within the pipe wall, and the thermophysical properties of the pipe material (electrical resistivity and thermal conductivity). In these calculations, axial conduction was assumed negligible, but peripheral and radial conduction of heat in the tube wall were included. In addition, the bulk fluid temperature was assumed to increase linearly from the inlet to outlet (see Fig. 4).

A National Instruments data acquisition system was used to record and store the data measured during these experiments. The acquisition system is housed in an AC powered four-slot SCXI 1000 Chassis that serves as a low noise environment for signal conditioning. Three NI SCXI control modules are housed inside the chassis. There are two SCXI 1102/B/C modules and one SCXI 1125 module. From these three modules, input signals for all 40 thermocouples, the two thermocouple probes, volt and current meters, and flow meters are gathered and recorded. The computer interface used to record the data is a LabVIEW Virtual Instrument (VI) program specifically written for this application.

The uncertainty analyses of the overall experimental procedures using the method of Kline and McClintock (1953) showed that there is a maximum of 11.5% uncertainty for the overall mean heat transfer coefficient calculations. Experiments under the same conditions were conducted periodically to ensure the repeatability of the results. The maximum difference between the duplicated experimental runs was within 10%. More details of experimental setup and data reduction procedures can be found from Durant (2003).

The heat transfer data obtained with the present experimental setup were measured under a uniform wall heat flux boundary condition that ranged from 2730 W/m^2 to 10,690 W/m^2 and the resulting overall mean two-phase heat transfer coefficients (h_{TP}) ranged from 513 W/(m^2 K) to 4419 W/(m^2 K). For these experiments, the liquid superficial Reynolds number (Re_{SL}) ranged from 821 to 26,043 (water mass flow rates from about 1.18 kg/min to 42.5 kg/min) and the gas superficial Reynolds numbers (Re_{SG}) ranged from 560 to 47,718 (gas mass flow rates from about 0.013 kg/min to 1.13 kg/min).

4. Experimental results

4.1. Flow patterns

Due to the multitude of flow patterns and the various interpretations accorded to them by different investigators, no uniform procedure exists at present for describing and classifying them. In this study, the flow pattern identification for the experimental data was based on the procedures suggested by Kim and Ghajar (2002), and visual observations deemed appropriate. All observations for the flow pattern judgments were made at two locations, just before the test section (about $L/D = 93$ in calming section from the air–water mixer) and right after the test section (see Fig. 1). Leaving the liquid flow rate fixed, flow patterns were observed for various air flow rates. The liquid flow rate was then adjusted and the process was repeated. If the observed flow patterns differed at the two locations of before and after the test section, experimental data was not taken and the flow rates of gas and liquid were readjusted for consistent flow pattern observations. These experimental data were plotted and compared using their corresponding values of mass flow rates of air and water and the flow patterns. The different flow patterns depicted in Fig. 5 illustrate the capability of our experimental setup in producing multitude of flow patterns. The shaded regions represent the boundaries of these flow patterns. Also shown in Fig. 5 with symbols is the distribution of the heat transfer data that were obtained systematically in our experimental setup with the pipe in the horizontal position. As can be seen from Fig. 5, we did not collect heat transfer data at low air and water flow rate combinations (water flow rates of less than about 5 kg/min and air flow rates of less than about 0.5 kg/min). At these low water and air flow rates and heating there is a strong possibility of either dryout or local boiling which could damage the test section. Fig. 6 shows photographs of the representative flow patterns that were observed in our experimental setup with the pipe in the horizontal position and no heating (isothermal runs).
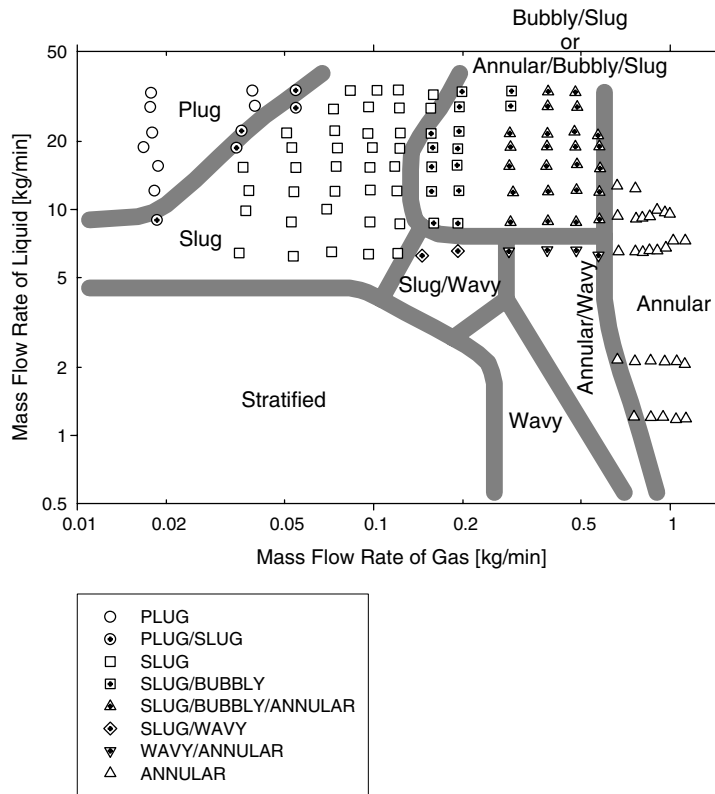
Fig. 5. Flow pattern map for horizontal flow.

4.2. Systematic investigation on two-phase heat transfer

As mentioned in Section 1, one of the objectives of this study was to systematically gather quality gas–liquid non-boiling flow heat transfer data for a variety of flow patterns in a horizontal pipe and use the data to better understand the non-boiling two-phase flow heat transfer behavior in horizontal pipes with respect to different flow patterns. In this section we present an overview of the different trends that we have observed in the heat transfer behavior of the two-phase air–water flow in a horizontal pipe for a variety of flow patterns. The two-phase heat transfer data were obtained by systematically varying the air or water flow rates.

Fig. 7 provides an overview of the pronounced influence of the flow pattern, superficial liquid Reynolds number (water flow rate) and superficial gas Reynolds number (air flow rate) on the overall mean two-phase heat transfer coefficient in horizontal pipe flow. The results presented in Fig. 7(a) clearly show that two-phase mean heat transfer coefficients are strongly influenced by the liquid superficial Reynolds number (Re_{SL}). As shown in the figure, the heat transfer coefficient increases proportionally as Re_{SL} increases. In addition, for a fixed Re_{SL}, the two-phase mean heat transfer coefficients are also influenced by the gas superficial Reynolds number (Re_{SG}), as shown in Fig. 7(b). However, the influence of Re_{SG} on the heat transfer coefficients is not as strong as that of Re_{SL}. The results shown in Fig. 7(b) also reveal that for each flow pattern, the heat transfer results have their own unique and repeatable behavior. Typically, heat transfer increases at low Re_{SG} (the regime of plug flow), and then slightly decreases at the mid range of Re_{SG} (the regime of slug and slug-type transitional flows), and again increases at the high Re_{SG} (the regime of annular flow).

In the next two sections we have provided additional insight to our heat transfer data by focusing on the two-phase heat transfer behavior of slug and annular flows. These are two commonly discussed flow patterns in the literature.
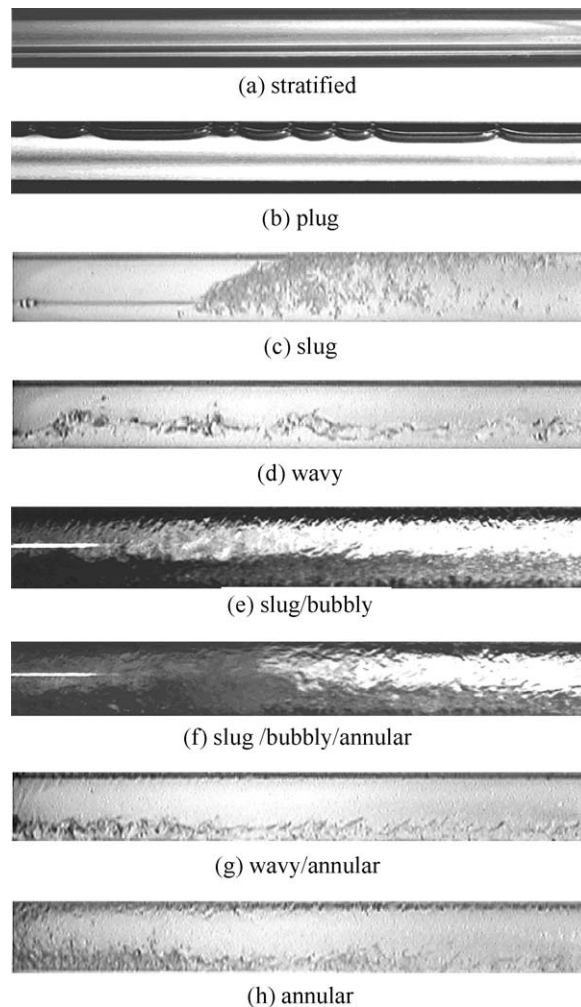
Fig. 6. Photographs of flow patterns (horizontal flow and isothermal).

4.2.1. Heat transfer behavior of slug flow

From Fig. 8(a) it can be observed again that the overall mean heat transfer coefficients substantially increase with the increase in Re_{SL} and Fig. 8(b) shows a slight decrease with the increase in Re_{SG} at a fixed Re_{SL} [the slug-type transition flows also show the same trend, see Fig. 7(b)]. Fig. 8 clearly indicates that the liquid phase is the dominant phase for heat transfer in slug flow and the effect of gas phase on heat transfer may be negligible. However, note that the average slope of h_{TP} data for a fixed Re_{SL} is -0.083 W/(m^2 K) over the range of Re_{SG} [see Fig. 8(b)] compared to an average slope $+0.196$ W/(m^2 K) for the h_{TP} data for a fixed Re_{SG} over the range of Re_{SL} [see Fig. 8(a)]. Therefore, the rate of decrease in h_{TP} with respect to Re_{SG} is about half of the rate of increase of h_{TP} with respect to Re_{SL} [0.083 W/(m^2 K) vs. 0.196 W/(m^2 K)]. This implies that an increase in Re_{SG} for a fixed Re_{SL} causes a fast drop in the overall mean heat transfer coefficient and its effect should not be ignored in the slug flow heat transfer analysis.

4.2.2. Heat transfer behavior of annular flow

From Fig. 7(b), discussed earlier, it can be seen that generally, as Re_{SL} increases for a fixed Re_{SG}, h_{TP} steadily increases for all the flow patterns. However, the reverse is not always true for all the flow patterns. As shown in Fig. 7(b) for the annular and annular-type flows, as Re_{SG} increases for a fixed Re_{SL}, the heat transfer coefficient increases, which is opposite of what was observed for the slug and slug-type flows discussed earlier.
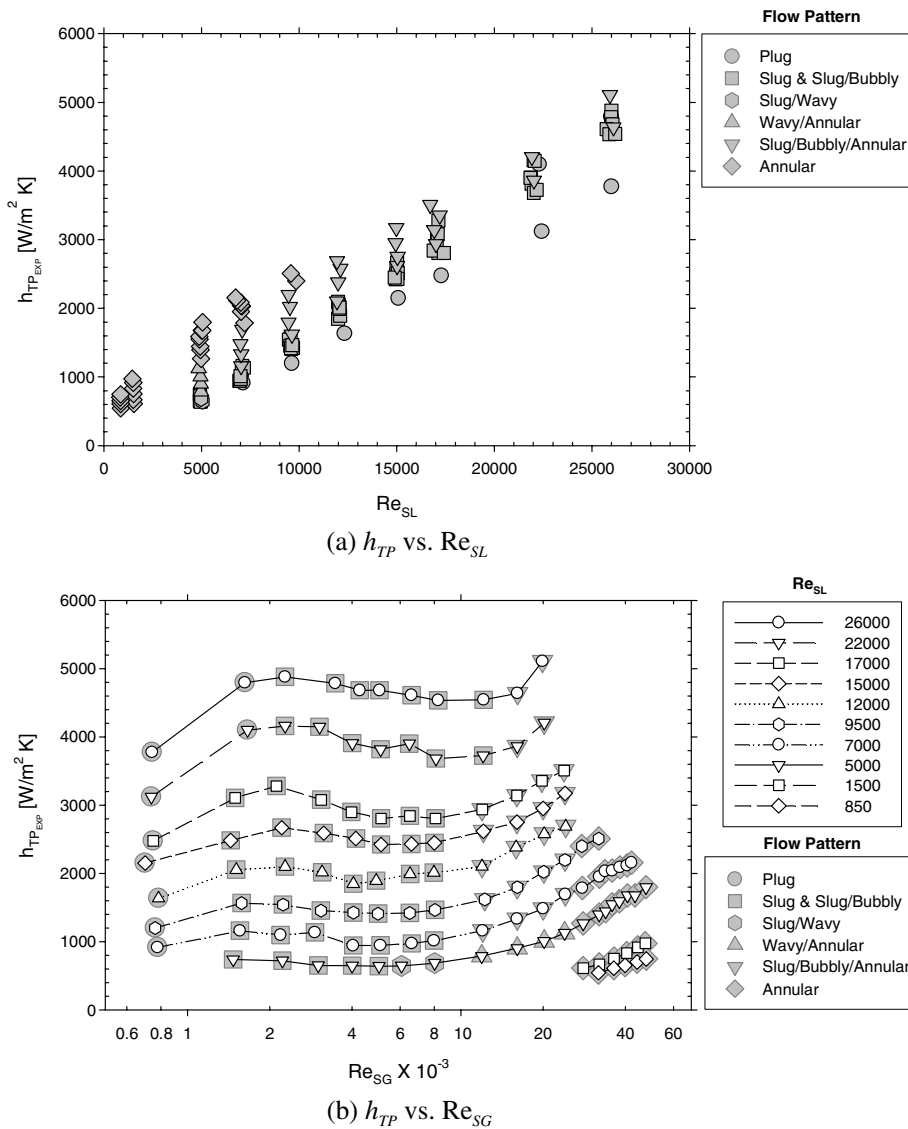
Fig. 7. Variation of h_{TP} for horizontal gas–liquid flow.

To get a better understanding of the heat transfer behavior in annular flow over a much wider range of Re_{SG} values, we also investigated Pletcher's (1966) annular flow data.

For Pletcher's (1966) annular flow experiments, Re_{SL} ranged from 1429 to 9776 and Re_{SG} varied from 33,344 to 293,140. The mean heat transfer coefficients for his experiments ranged from 2331 to 8016 W/(m^2 K). Our data and his data cannot be compared directly since his values of Re_{SG} were much larger than ours ($Re_{SG} \approx 550$–48,000), but his Re_{SL} fell within the same range as our experiments ($Re_{SL} \approx 800$–26,000).

The heat transfer results from Pletcher (1966) can be considered as an extension of our annular flow heat transfer results and can be used to establish the heat transfer behavior of annular flow in horizontal pipes over a relatively low to moderate range of Re_{SL} and relatively low to very high range of Re_{SG}. For this reason the results of our study were combined with Pletcher's (1966) data and plotted as shown in Fig. 9. This figure gives a complete representation of the heat transfer behavior of annular flow over a wide range of superficial Reynolds numbers. From Fig. 9 it can be observed that the mean two-phase heat transfer coefficients substantially
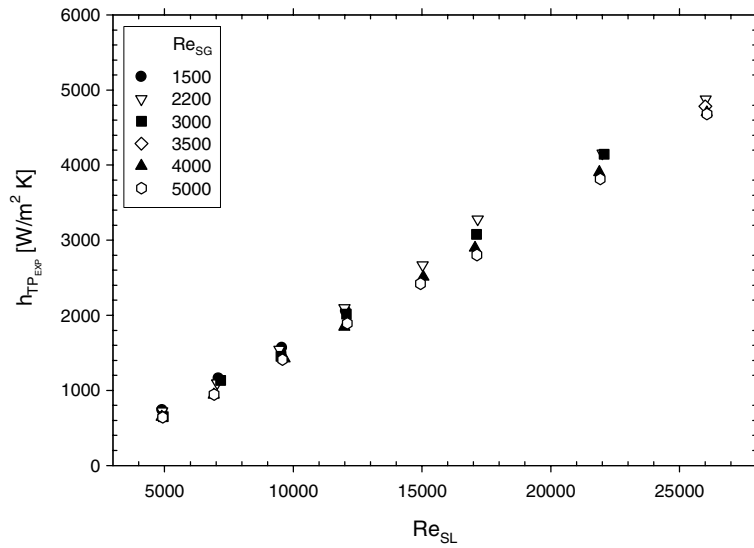
(a) h_{TP} vs. Re_{SL}
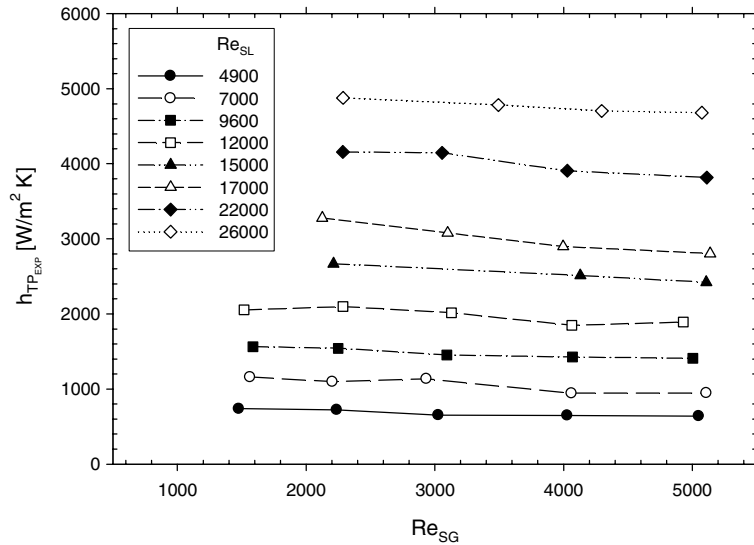
(b) h_{TP} vs. Re_{SG}

Fig. 8. Variation of h_{TP} for slug flow in a horizontal pipe.

increase with the increase in Re_{SL}, and show a slight increase with the increase in Re_{SG} until Re_{SG} becomes too large ($\approx 10^5$). At large values of Re_{SG}, according to Pletcher (1966), evaporation and entrainment became the dominating factors thus causing the mean heat transfer coefficients to decrease.

In regard to Pletcher's (1966) heat transfer data, for the very high flow rates of air used in his experiments (Re_{SG} varied from 33,344 to 293,140) there is a strong possibility that dryout could have occurred in his test pipe. Dryout is an occurrence of two-phase flow where the liquid is blown away from the medium wall because of high gas flow rates. This would then cause abnormal heating, resulting in poor heat transfer coefficient measurements. Pletcher's (1966) method of verifying the absence of dryout is unknown. In our experiments dryout was avoided by visually observing the flow at the entrance and exit of the pipe to verify that the pipe walls were wetted as the annular flow passed through the pipe.
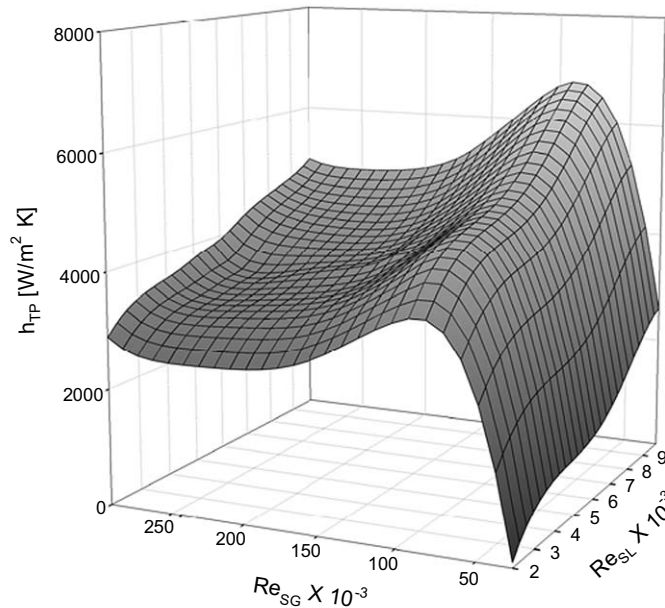
Fig. 9. Variation of h_{TP} for annular flow in horizontal pipes.

5. Development of the general heat transfer correlation

The last objective of this study was to use the detailed knowledge gained through our systematic two-phase flow heat transfer measurements and develop a robust heat transfer correlation to predict non-boiling two-phase flow heat transfer in horizontal pipes for a variety of flow patterns. For this purpose we will build on our previous work (Kim et al., 2000; Kim and Ghajar, 2002).

Kim et al. (2000) in the development of their heat transfer correlation, Eq. (1), assumed the total heat transfer in gas–liquid flow to be the sum of the individual single-phase heat transfers of the gas and liquid, weighted by the volume of each phase present. Based on their assumption, the mean two-phase heat transfer coefficient was expressed as

$$h_{TP} = (1 - \varepsilon)h_L + \varepsilon h_G \tag{3}$$

where h_G is heat transfer coefficient for gas (evaluated as if only gas phase alone were flowing).

Based on this assumption Kim et al. (2000) developed their heat transfer correlation, Eq. (1). The performance of Eq. (1) was discussed in Section 2 and it was pointed out that the heat transfer correlation is not capable of predicting the two-phase heat transfer data in horizontal pipes for all the different flow patterns with the same set of constants. In other words, the correlation was not capable of properly accounting for the effect of different flow patterns on the two-phase heat transfer. To remedy this situation, the weighting factors assigned to h_L and h_G in Eq. (3) should be revisited. This will be presented next.

5.1. Void fraction as a weighting factor in the correlation

The importance of knowing how much of a pipe is occupied by each phase of a gas–liquid flow is obvious if the general differences of the heat transfer capabilities between liquid and gas are considered. The evaluation of how much of a pipe cross-sectional area is wetted is fairly straightforward and can be done by using the relationship between void fraction and channel dimensions as shown below.

The hydraulic diameter occupied by the liquid phase (D_L) can be evaluated as

$$D_L = \frac{4A_L}{S_L} \tag{4}$$

where A_L is the cross-sectional area of the pipe occupied by the liquid phase and S_L is the wetted-perimeter by the liquid phase.

Substituting $A_L = (1 - \varepsilon)A$ into Eq. (4), the wetted-perimeter at the equilibrium (static) state, $S_{L,eq}$ [refer to Fig. 10(a)], in the non-dimensionalized form $(\widetilde{S}_{L,eq})$, becomes

$$\widetilde{S}_{L,eq}^2 = \left(\frac{S_{L,eq}}{\pi D}\right)^2 = (1 - \varepsilon) \tag{5}$$

Referring to Eq. (5), it seems reasonable that the void fraction term $(1 - \varepsilon)$, which is a very popular parameter in gas–liquid flow, to be used as a weighting factor in the development of two-phase heat transfer correlations as was done in Eq. (3). However, as shown in Fig. 10, $(1 - \varepsilon)$ does not properly represent the interaction between the two phases in a gas–liquid flow and a different weighting factor should be considered to represent the actual amount of heat transfer by the liquid and gas phases in a horizontal flow.

In horizontal gas–liquid flow, it is well-known that distinguishable flow patterns exist (see Fig. 6) due to the complex interaction between the momentum forces and the differences in the buoyancy force of each phase. Therefore, to properly account for the heat transfer contribution of each phase, the different cross-sectional flow shapes (wetted-perimeter) of gas–liquid flow for each flow pattern must be considered. However, the term $(1 - \varepsilon)$, which is the squared non-dimensionalized wetted-perimeter evaluated at the equilibrium state $(\widetilde{S}_{L,eq}^2)$, does not reflect the actual interface shape of the flow and as a result, it cannot see any differences between the different flow patterns as shown in Fig. 10(a). In the next section, a new weighting factor, referred to as the flow pattern factor (F_P) is developed to properly account for the heat transfer contributions of gas and liquid phases in different flow patterns.
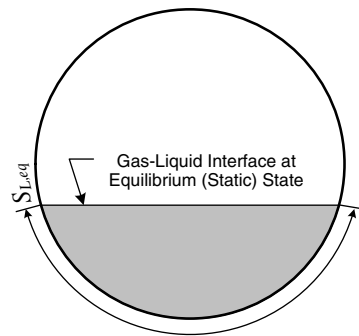
(a) equilibrium state
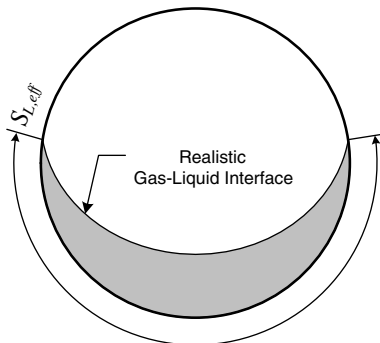
(b) realistic (effective) interface

Fig. 10. Gas–liquid interfaces and wetted-perimeters.

5.2. Flow pattern factor (effective wetted-perimeter relation)

As discussed in the previous section, the void fraction term, $(1 - \varepsilon)$ does not reflect the actual wetted-perimeter (S_L) in the pipe with respect to the corresponding flow pattern in horizontal flow as shown in Fig. 10. For instance, $(1 - \varepsilon)$ and $\widetilde{S}_L$ of plug flow both approach unity, but in the case of annular flow $(1 - \varepsilon)$ is near zero and $\widetilde{S}_L$ is near unity. Therefore, as discussed in the previous section, S_L must be considered as a weighting factor instead of the void fraction term in order to properly account for the effect of different flow patterns. However, the estimation of the actual wetted-perimeter (S_L) is very difficult due to the continuous interaction between the two phases in gas–liquid flow. Therefore, instead of estimating the actual wetted-perimeter (S_L), modeling the effective wetted-perimeter ($S_{L,eff}$) may be a more practical approach [refer to Fig. 10(b)]. Note that in our model we have neglected the influence of the surface tension and the contact angle of each phase on the evaluation of the effective wetted-perimeter.

In order to capture the realistic shape of the gas–liquid interface, the flow pattern factor (F_P), an effective wetted-perimeter ($S_{L,eff}$) relation, which is a modified version of the equilibrium wetted-perimeter ($S_{L,eq}$), Eq. (6), is proposed

$$F_P = \widetilde{S}_{L,eff}^2 = \left(\frac{S_{L,eff}}{\pi D}\right)^2 = (1 - \varepsilon) + \varepsilon F_S^2 \tag{6}$$

where in the above equation for simplicity the effective wetted-perimeter relation ($\widetilde{S}_{L,eff}^2$) is referred to as the flow pattern factor (F_P). The term F_S appearing in Eq. (6) is referred to as shape factor which in essence is a modified and normalized Froude number. The shape factor (F_S) is defined as

$$F_S = \frac{2}{\pi} \tan^{-1}\left(\sqrt{\frac{\rho_G(u_G - u_L)^2}{gD(\rho_L - \rho_G)}}\right) \tag{7}$$

where ρ is density, g is acceleration due to gravity, and u_L and u_G are mean velocities of liquid and gas and evaluated by $u_L = \dot{m}_L/[\rho_L(1 - \varepsilon)A]$ and $u_G = \dot{m}_G/(\rho_G \varepsilon A)$, respectively.

The shape factor (F_S) is applicable for slip ratios $K (= u_G/u_L) \geqslant 1$, which is common in gas–liquid co-current flows, and represents the shape changes of the gas–liquid interface by the force acting on the interface due to the relative momentum and gravity forces.

5.3. Heat transfer data response to flow pattern factor

In the previous section, we developed a flow pattern factor (F_P) in order to handle the various flow patterns in gas–liquid horizontal pipe flow. Here, we have presented the response of the proposed flow pattern factor to our experimental data.

The response of the flow pattern factor to our data is shown in Figs. 11 and 12. In Fig. 11 we have plotted Eqs. (5) and (6) against the Martinelli parameter as defined by Lockhart and Martinelli (1949), $X = [(dp/dz)_L/(dp/dz)_G]^{0.5}$ where dp/dz is the pressure drop in the axial direction. From this figure it is evident that the flow pattern factor (F_P) is clearly separated from the equilibrium wetted-perimeter $(1 - \varepsilon)$ as the flow patterns change from plug to annular. This distinct separation between the flow patterns shown in Fig. 11 proves that the proposed flow pattern factor does an excellent job of distinguishing between the different flow patterns. Obviously this was not the case when the equilibrium wetted-perimeter relation $(1 - \varepsilon)$ was used. In Fig. 12 the weighted liquid-alone heat transfer coefficients (h_L) are plotted vs. the experimentally obtained two-phase flow heat transfer coefficients (h_{TP}). Here we see that by using F_P as the weighting factor, the experimental heat transfer data all collapsed into one single curve and were very well represented. As shown in Fig. 12 with the use of equilibrium wetted-perimeter relation $(1 - \varepsilon)$, the experimental data showed a very strong dependency on the flow pattern and were not well represented at all.

The results presented in Figs. 11 and 12 demonstrate that our proposed flow pattern factor is capable of handling the effects of different flow patterns. Based on these findings, we will next propose a new general
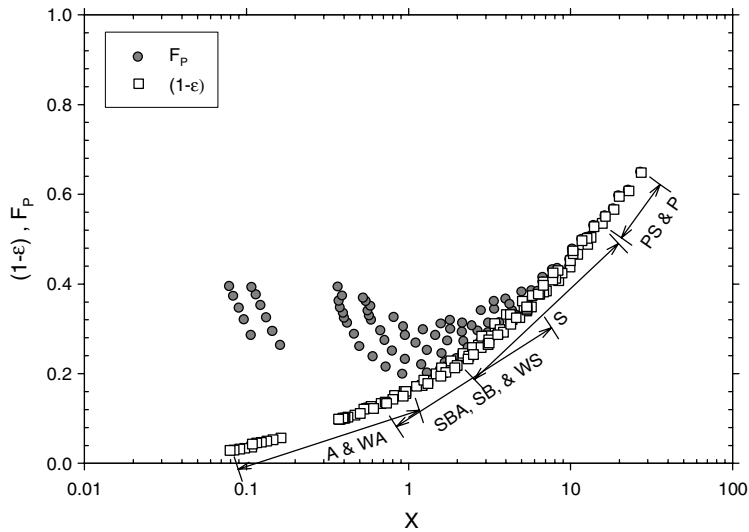
Fig. 11. Equilibrium wetted-perimeter $(1 - \varepsilon)$ and the flow pattern factor (F_P) for the horizontal flow experimental data (A: annular flow, WA: wavy/annular flow, SBA: slug/bubbly/annular flow, SB: slug/bubbly flow, WS: wavy/slug flow, S: slug flow, PS: plug/slug flow, and P: plug flow).
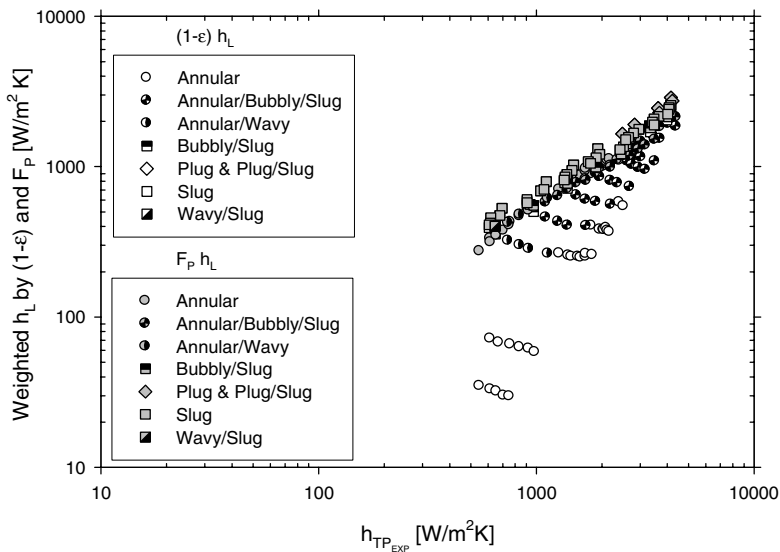

Fig. 12. Weighted h_L by $(1 - \varepsilon)$ and F_P for the horizontal flow experimental data.

correlation that is capable of predicting non-boiling two-phase flow heat transfer in horizontal pipes for a variety of flow patterns.

5.4. Heat transfer correlation

Introduce the proposed flow pattern factor (F_P) into the two-phase heat transfer correlation, Eq. (1). Substitute F_P for $(1 - \varepsilon)$, the weighting factor for h_L, and replace the void fraction ratio $[\varepsilon/(1 - \varepsilon)]$ with $[(1 - F_P)/F_P]$. With these substitutions the new form of Eq. (1) is

$$h_{\text{TP}} = F_{\text{P}} h_{\text{L}} \left\{ 1 + C \left[\left(\frac{x}{1-x} \right)^m \left(\frac{1-F_{\text{P}}}{F_{\text{P}}} \right)^n \left(\frac{Pr_{\text{G}}}{Pr_{\text{L}}} \right)^p \left(\frac{\mu_{\text{G}}}{\mu_{\text{L}}} \right)^q \right] \right\} \tag{8}$$

where h_{L} comes from the Sieder and Tate (1936) correlation for turbulent flow given as

$$h_{\text{L}} = 0.027 Re_{\text{L}}^{4/5} Pr_{\text{L}}^{1/3} \left(\frac{k_{\text{L}}}{D} \right) \left(\frac{\mu_{\text{B}}}{\mu_{\text{W}}} \right)_{\text{L}}^{0.14} \tag{9}$$

For the Reynolds number needed in the h_{L} calculations, the following relationship is used to evaluate the in-situ Reynolds number (liquid phase, Re_{L}) rather than the superficial Reynolds number (Re_{SL}) as commonly used in the correlations available in the literature (see Kim et al., 1999)

$$Re_{\text{L}} = \left(\frac{\rho u D}{\mu} \right)_{\text{L}} = \frac{4\dot{m}_{\text{L}}}{\pi \sqrt{1-\varepsilon} \mu_{\text{L}} D} \tag{10}$$

In this study the values of the void fraction used in Eqs. (8) and (10) are calculated based on the correlation proposed by Chisholm (1983), which can be expressed as

$$\varepsilon = \left[1 + \left(\frac{\rho_{\text{L}}}{\rho_{\text{m}}} \right)^{0.5} \left(\frac{1-x}{x} \right) \left(\frac{\rho_{\text{G}}}{\rho_{\text{L}}} \right) \right]^{-1} \tag{11}$$

where $1/\rho_{\text{m}} = (1-x)/\rho_{\text{L}} + (x/\rho_{\text{G}})$.

Note that any other reliable correlation for void fraction or single-phase turbulent heat transfer could have been used in place of Chisholm (1983) and the Sieder and Tate (1936) correlations, respectively. The difference resulting from the use of the different correlations will be absorbed in the values of different constants (C, m, n, p, q) of Eq. (8).

5.5. Determination of the constants in the proposed correlation

To determine the values of the constants (C, m, n, p, q) in Eq. (8), a total of 114 horizontal pipe flow experimental data points of Ghajar et al. (2004a,b,c) were used (28 points for annular flow; 36 points for slug flow; and 50 points for plug and transitional flow). Table 2 and Fig. 13(a) provide the details of the correlation and how well the proposed correlation predicted the experimental data. The correlation predicted the experimental data with an overall mean deviation of 5.5% and a standard deviation of 11.7%. Ninety three percent (93%) of the data points were predicted within ±20% deviation.

For an independent validation of our proposed heat transfer correlation with the determined constants, we tested its predictive capabilities with the experimental data of Kim and Ghajar (2002). Their data was briefly discussed in reference to Table 1. To properly use their experimental data in our proposed heat transfer correlation, the overall mean two-phase heat transfer coefficients (h_{TP}) for their data were obtained based on Eq. (2) rather than averaging all 40 local heat transfer coefficients in the test section, as suggested by Kim and Ghajar (2002). As shown in Fig. 13(b), our proposed correlation with the determined constants predicted

Table 2
Determined constants, prediction results, and range of parameters for Eq. (8)

Experiment (no. of data points)	Value of constants					Prediction statistics				Range of parameters				
	C	m	n	p	q	Mean dev. (%)	Std. dev. (%)	Range of dev. (%)	Number of data points	Re_{SL}	F_{P}	x	$\left(\frac{Pr_{\text{G}}}{Pr_{\text{L}}}\right)$	$\left(\frac{\mu_{\text{G}}}{\mu_{\text{L}}}\right)$
Current study (114 data points)	0.7	0.08	0.06	0.03	−0.14	5.5	11.7	−18.3 to 37.0	106 within ±20%	835 to 25931	0.198 to 0.648	1.16×10^{-3} to 0.487	0.092 to 0.110	0.016 to 0.020
Kim and Ghajar (2002) except wavy flow (130 data points)						−13.6	18.2	−45.3 to 36.5	108 within ±30%	2163 to 35503	0.226 to 0.735	6.85×10^{-4} to 0.115	0.091 to 0.136	0.015 to 0.028
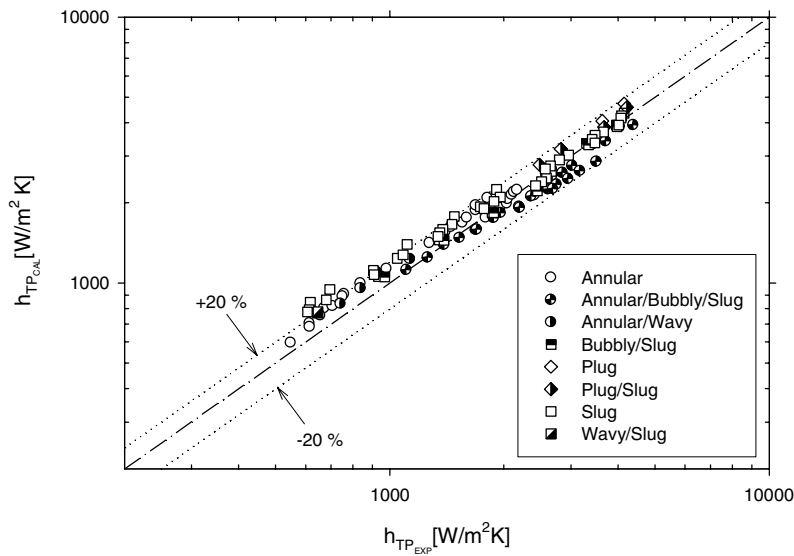
(a) data from current study (114 data points)
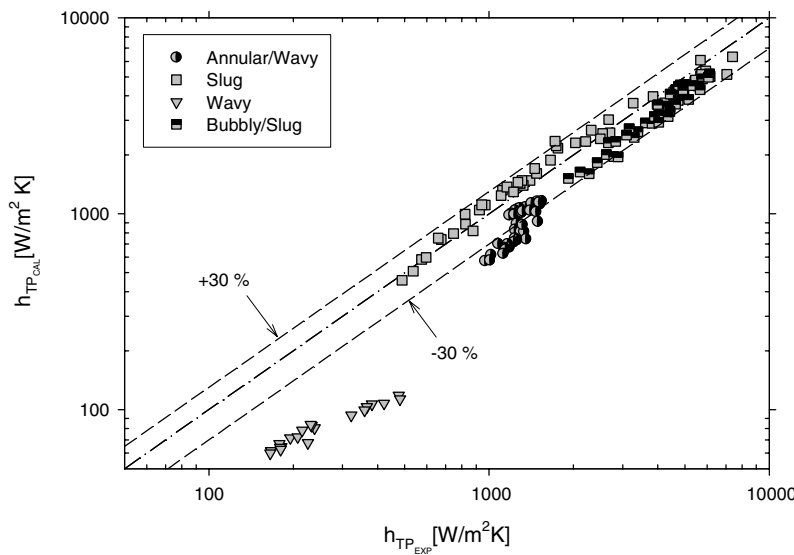
(b) data from Kim and Ghajar (2002) (150 data points)

Fig. 13. Comparison of the predictions of the proposed correlation with experimental data.

the overall mean two-phase heat transfer coefficients very well, except for the wavy flow data. The proposed correlation predicted the experimental data (with the exception of the wavy flow data) of Kim and Ghajar (2002) with an overall mean deviation of -13.6% and a standard deviation of 18.2%. Eighty three percent (83%) of the data points were predicted within $\pm30\%$ deviation. The details of how well the correlation predicted the experimental data of Kim and Ghajar (2002) is also provided in Table 2.

The reason our proposed correlation did not do well in predicting the wavy flow data of Kim and Ghajar (2002) is because of the uncharacteristic heat transfer behavior displayed by their data. Further analysis of their data showed that the ratio of the bottom to top local heat transfer coefficients ($h_{\text{bottom}}/h_{\text{top}}$) ranged from 58 to 346 with an average h_{top} of only 11 W/(m² K) for all the 20 wavy flow data points. The data indicates that on the average about 92% of the heat transfer is through the bottom part of the pipe. This strong unbalanced circumferential heat transfer behavior in the wavy flow data of Kim and Ghajar (2002) points to the

strong possibility of the presence of dryout or near dryout in the top part of their test pipe during the wavy flow experiments. Hence, our proposed correlation under predicted their experimental data.

These results provide additional validation on the robustness of the general two-phase heat transfer correlation proposed by Kim et al. (2000). In addition, the modifications made to the general heat transfer correlation to account for the various flow patterns appear to be correct.

6. Conclusions

The purpose of this study was to further develop the knowledge and understanding of heat transfer in non-boiling two-phase, two-component, gas–liquid flow. For this purpose systematic air–water flow heat transfer experiments were conducted in a circular pipe in the horizontal position under uniform wall heat flux boundary condition.

The results showed that the two-phase flow heat transfer rate proportionally increased as Re_{SL} increased. For a fixed Re_{SL} the heat transfer results showed distinguished trends depending on the flow pattern and Re_{SG}. In general our systematic heat transfer results revealed that the relationship between Re_{SL}, Re_{SG}, and flow pattern is very complicated.

This study also led to the development of a general heat transfer coefficient correlation for horizontal gas–liquid flow for different flow patterns. In order to properly account for the effect of different flow patterns on the heat transfer in gas–liquid flow in a horizontal pipe, a flow pattern factor (F_P) was developed and introduced into our previously developed heat transfer correlation. The data collected in this study for different flow patterns were successfully predicted by the proposed general heat transfer correlation.

Acknowledgements

References

Chisholm, D., 1983. Two-phase flow in pipelines and heat exchangers. In: George Godwin (Ed.), London and New York in association with the Institution of Chemical Engineers, New York.

Durant, W.B., 2003. Heat transfer measurement of annular two-phase flow in horizontal and a slightly upward inclined tube. M.S. Thesis, Oklahoma State University, Stillwater, OK.

Ghajar, A.J., Kim, J., 2006. Calculation of local inside-wall convective heat transfer parameters from measurements of the local outside-wall temperatures along an electrically heated circular tube. In: Kutz, M. (Ed.), Heat Transfer Calculations. McGraw-Hill, New York, pp. 233–2327 (Chapter 23).

Ghajar, A.J., Zurigat, Y.H., 1991. Microcomputer-assisted heat transfer measurement/analysis in a circular tube. Int. J. Appl. Eng. Educat. 7, 125–134.

Ghajar, A.J., Kim, J., Durant, W.B., Trimble, S.A., 2004a. An experimental study of heat transfer in annular two-phase flow in a horizontal and slightly upward inclined tube. In: HEFAT2004: Proceedings of the 3rd International Conference on Heat Transfer, Fluid Mechanics and Thermodynamics, 21–24 June, Cape Town, South Africa, Paper No. GA1.

Ghajar, A.J., Kim, J., Malhotra, K., Trimble, S.A., 2004b. Systematic heat transfer measurements for air–water two-phase flow in a horizontal and slightly upward inclined pipe. In: ENCIT2004: Proceedings of the 10th Brazilian Congress of Thermal Sciences and Engineering, November 29–December 3, Rio de Janeiro, Brazil, Paper No. CIT04–0471.

Ghajar, A.J., Malhotra, K., Kim, J., Trimble, S.A., 2004c. Heat transfer measurements and correlations for air–water two-phase slug flow in a horizontal pipe. In: HT-FED2004: Proceedings of the 2004 ASME Heat Transfer/Fluids Engineering Summer Conference, July 11–15, Charlotte, North Carolina, Paper No. HT-FED2004–56614.

Kim, D., Ghajar, A.J., 2002. Heat transfer measurements and correlations for air–water flow of different flow patterns in a horizontal pipe. Exp. Thermal Fluid Sci. 25, 659–676.

Kim, D., Ghajar, A.J., Dougherty, R.L., Ryali, V.K., 1999. Comparison of 20 two-phase heat transfer correlations with seven sets of experimental data, including flow pattern and tube inclination effects. Heat Transfer Eng. 20, 15–40.

Kim, D., Ghajar, A.J., Dougherty, R.L., 2000. Robust heat transfer correlation for turbulent gas–liquid flow in vertical pipes. J. Thermophys. Heat Transfer 14, 574–578.

King, C.D.G., 1952. Heat transfer and pressure drop for an air–water mixture flowing in a 0.737 inch I.D. horizontal tube. M.S. Thesis, University of California, Berkeley, CA.

Kline, S.J., McClintock, F.A., 1953. Describing uncertainties in single-sample experiments. Mech. Eng. 75, 3–8.

Lockhart, R.W., Martinelli, R.C., 1949. Proposed correlation of data for isothermal two-phase, two-component flow in pipes. Chem. Eng. Prog. 45, 39–48.

Pletcher, R.H., 1966. An experimental and analytical study of heat transfer and pressure drop in horizontal annular two-phase, two-component flow. Ph.D. Thesis, Cornell University, Ithaca, NY.

Sieder, E.N., Tate, G.E., 1936. Heat transfer and pressure drop of liquids in tubes. Indus. Eng. Chem. 28, 1429–1435.